Fraunhofer Institut
Techno- und
Wirtschaftsmathematik

O. Wirjadi

Survey of 3d image segmentation methods

Berichte des Fraunhofer ITWM, Nr. 123 (2007)

ISSN 1434-9973

Bericht 123 (2007)

Die Veröffentlichungen in der Berichtsreihe des Fraunhofer ITWM können bezogen werden über:

Fraunhofer-Institut für Techno- und
Wirtschaftsmathematik ITWM
Fraunhofer-Platz 1

67663 Kaiserslautern
Germany

Telefon: +49(0)631/31600-0
Telefax: +49(0)631/31600-1099
E-Mail: info@itwm.fraunhofer.de
Internet: www.itwm.fraunhofer.de

Vorwort

Das Tätigkeitsfeld des Fraunhofer-Instituts für Techno- und Wirtschaftsmathematik ITWM umfasst anwendungsnahe Grundlagenforschung, angewandte Forschung sowie Beratung und kundenspezifische Lösungen auf allen Gebieten, die für Techno- und Wirtschaftsmathematik bedeutsam sind.

In der Reihe »Berichte des Fraunhofer ITWM« soll die Arbeit des Instituts kontinuierlich einer interessierten Öffentlichkeit in Industrie, Wirtschaft und Wissenschaft vorgestellt werden. Durch die enge Verzahnung mit dem Fachbereich Mathematik der Universität Kaiserslautern sowie durch zahlreiche Kooperationen mit internationalen Institutionen und Hochschulen in den Bereichen Ausbildung und Forschung ist ein großes Potenzial für Forschungsberichte vorhanden. In die Berichtreihe sollen sowohl hervorragende Diplom- und Projektarbeiten und Dissertationen als auch Forschungsberichte der Institutsmitarbeiter und Institutsgäste zu aktuellen Fragen der Techno- und Wirtschaftsmathematik aufgenommen werden.

Darüber hinaus bietet die Reihe ein Forum für die Berichterstattung über die zahlreichen Kooperationsprojekte des Instituts mit Partnern aus Industrie und Wirtschaft.

Berichterstattung heißt hier Dokumentation des Transfers aktueller Ergebnisse aus mathematischer Forschungs- und Entwicklungsarbeit in industrielle Anwendungen und Softwareprodukte – und umgekehrt, denn Probleme der Praxis generieren neue interessante mathematische Fragestellungen.

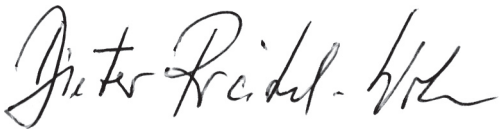

Prof. Dr. Dieter Prätzel-Wolters
Institutsleiter

Kaiserslautern, im Juni 2001

Survey of 3D Image Segmentation Methods

Oliver Wirjadi

Models and Algorithms in Image Processing
Fraunhofer ITWM, Kaiserslautern

Abstract

This report reviews selected image binarization and segmentation methods that have been proposed and which are suitable for the processing of volume images. The focus is on thresholding, region growing, and shape–based methods. Rather than trying to give a complete overview of the field, we review the original ideas and concepts of selected methods, because we believe this information to be important for judging when and under what circumstances a segmentation algorithm can be expected to work properly.

Keywords: image processing, 3D, image segmentation, binarization

Contents

1 Introduction

This report is intended to give a wide, but by no means complete, overview over common binarization and segmentation methods encountered in three dimensional image processing. We discuss gray-value, region, and shape based methods. To do this, we describe some algorithms which we believe to be representative for each class in some detail. We try to give an understanding of the original derivation and motivation of each algorithm, instead of merely stating how each method functions. We believe that this is of high importance in order to get an idea where and under what circumstances a method can function and when one can expect an algorithm to fail.

Of course, there already exist many reviews on image segmentation: Pal and Pal [PP93], which does not go into the details of the algorithms, but which classifies segmentation techniques, discusses advantages and disadvantages of each class of segmentation method and contains an exhaustive list of references to the literature up to the early 1990's. Trier and Jain [TJ95] review 11 locally adaptive binarizations algorithms and present a comparative evaluation for an optical character recognition (OCR) task in 2D. Another review that focuses on medical image segmentation can be found in [PXP00].

To briefly motivate why one should consider different 3D segmentation algorithms, consider the example of a 3D dataset in Fig. 1. Simple global thresholding, thoroughly defined below, can be used to mark the locations of fibers in this dataset, c.f. Fig. 1(e). But the individual fiber areas (indicated in black) are not separated, making it impossible to identify the exact extent of individual fibers in this image. By choosing different binarization parameters (Figures 1(c) and 1(d)), separation of the fibers can be improved, but this goes along with loosing some information within the fibers. All segmentation methods that have been proposed in the literature aim at improving image segmentation in this or other aspects. The causes for problems such as the ones in Fig. 1 can by manifold, many times being inherent to the respective image acquisition method itself.

1.1 Notation

Throughout this survey, we have 3D volume images in mind, such as they are produced by CT (x–ray computed tomography), MRI (magnetic resonance imaging), or others. An image f is defined over its image domain Ω as

$$f(\mathbf{x}) \in \mathbb{R}, \tag{1}$$

$$\mathbf{x} \in \Omega. \tag{2}$$

For the purposes of this survey, we can think of Ω as a discrete three dimensional space, indexing the grid points (voxels) on which gray values $f(\mathbf{x})$ are observed. A segmented image is denoted by g on the same domain Ω as the original image f, but taking on values from a discrete label space,

$$g(\mathbf{x}) \in \mathbb{N}. \tag{3}$$

Binary images are a special case of this definition, for they are restricted to values 0 and 1, indicating image background and foreground, respectively. The only exception from this convention will be Sec. 5.4. For the derivations of some of the methods, we will also need to be able to treat images as random processes. We use capital letters for random variables, such as $F(\mathbf{x})$ at voxel $\mathbf{x}$, and we use p to denote a probability density function. As is common, we write $p(f)$ as shorthand notation for $p_F(F = f)$, the joint distribution of all voxel values.

Other concepts that will be used throughout this text are related to the discrete grid Ω over which images f or g are defined: A neighbor of a voxel $\mathbf{x}$ is a voxel $\mathbf{x}'$ that is adjacent to $\mathbf{x}$ with respect to some neighborhood definition. Two common definitions in 3D are 6 and 26 neighborhoods, i.e., voxels are neighbors if they have a common face, or if they have a common face, edge or vertex, respectively. We will write $N(\mathbf{x})$ for the set of all neighbors of $\mathbf{x}$. A connected region or component is then a set of voxels in which any two elements can be connected by consecutive neighbors that are all contained in that set, themselves. A segment is what we like to achieve by segmentation, i.e., an image region that encloses the information of interest (e.g., an interesting microstructure or some defect in the image). Note that the definition of a segment that we make here is not a rigorous one, because its exact definition depends on how we compute the segment.

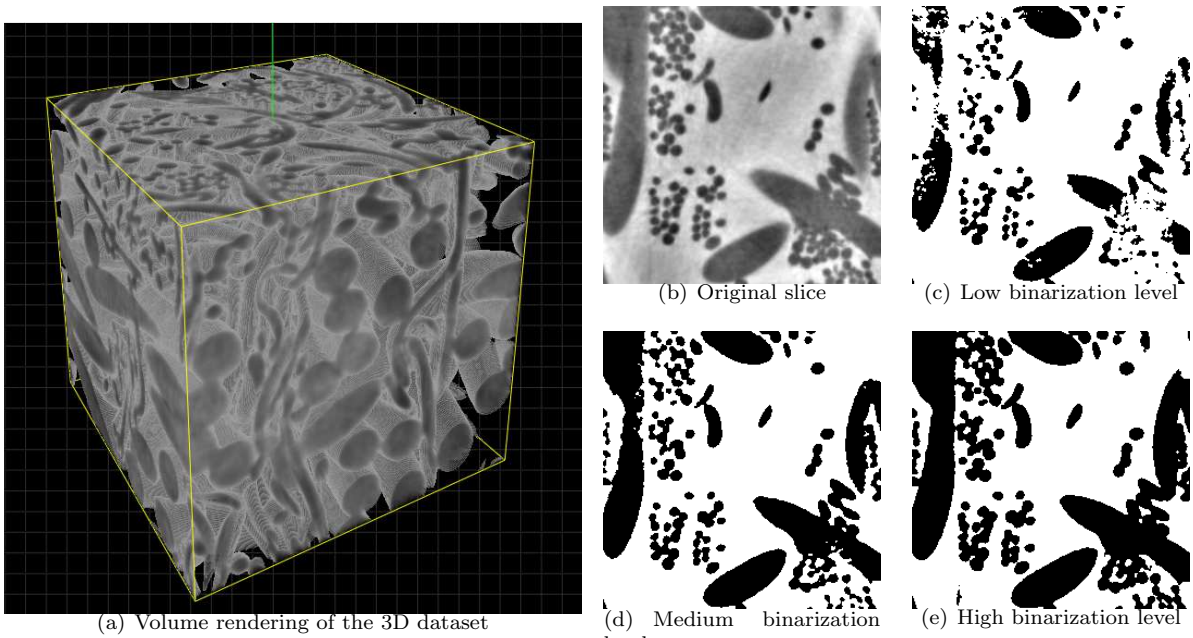

(a) Volume rendering of the 3D dataset

(b) Original slice

(c) Low binarization level

(d) Medium binarization level

(e) High binarization level

Figure 1: Examplary segmentations of a fiber felt (polyamid fibers): Even at low noise levels, separation of foreground can be difficult (data acquisition by L. Helfen / ESRF Grenoble, visualization by T. Sych / Fraunhofer ITWM).

2 Thresholding

There exists a large number of gray-level based segmentation methods using either global or local image information. In thresholding, one assumes that the foreground can be characterized by its brightness, which is often a valid assumption for 3D datasets.

2.1 Global Thresholding

This is the simplest and most widely used of all possible segmentation methods. One selects a value θ, $\min_{\mathbf{x}}(f(\mathbf{x})) \leq \theta \leq \max_{\mathbf{x}}(f(\mathbf{x}))$, and sets foreground voxels, accordingly.

$$g(\mathbf{x}) = \begin{cases} 1 & \text{if } f(\mathbf{x}) \geq \theta \\ 0 & \text{else} \end{cases} \tag{4}$$

While (4) is a complete description of a binarization algorithm, it contains no indication on how to select the value θ. The natural question that arises is whether there exists an optimal threshold value. There are in fact different solutions to this threshold selection problem, each being based on different model assumptions. We discuss some of these methods in the remainder of this section.

However, even if θ was optimally selected using a model which is suitable for the present image data, global thresholding will give poor results whenever influences of noise are large compared to the image content (low signal to noise ratio) or when object and background gray value intensities are not constant throughout the volume.

2.1.1 Choosing Thresholds Using Prior Knowledge

In many situations, an imaged object will have known physical properties. For example, the manufacturer of a material may know the material's volume density from experiments. Then, the optimal threshold θ^* may be defined as the value for which the segmented image g reaches this a–priorily known value. Such strategies can actually be applied for choosing parameters of any kind of image processing method.

For low noise levels and suitable known parameters, i.e., parameters which can also be computed from binarized images, this pragmatic approach can often yield satisfactory results, especially if combined with proper filtering methods for noise reduction.

2.1.2 Otsu's Method

For choosing θ, one can analyze the distribution of gray values of an image (its histogram): Assume that the gray value histogram of the image contains two separate peaks, one each for fore- and background voxels (bimodal histogram). Then we would want to choose the minimum between these two peaks as threshold θ. Otsu defines this choice for θ as the value minimizing the weighted sum of within-class variances [Ots79]. This is equivalent to maximizing the between-class scatter. For an image taking on discrete voxel values k, the optimal threshold is

$$\theta_{\text{Otsu}} = \text{argmax}_\theta \left\{ \sum_{k<\theta} p(k) \left(\mu_0 - \mu\right)^2 + \sum_{k \geq \theta} p(k) \left(\mu_1 - \mu\right)^2 \right\} \tag{5}$$

where

$$\begin{aligned} p &\quad \text{is the normalized histogram} \\ \mu &:= \text{Mean}\{f(\mathbf{x})\} \\ \mu_1 &:= \text{Mean}\{f(\mathbf{x}) \mid f(\mathbf{x}) \geq \theta\} \\ \mu_0 &:= \text{Mean}\{f(\mathbf{x}) \mid f(\mathbf{x}) < \theta\}. \end{aligned}$$

In the simple case of 256 gray values, T can be simply determined by evaluating the term for each value and choosing the global minimum. Note that, in the discrete case, (5) can be entirely evaluated from the histogram by summing over the appropriate value ranges. Otsu's method is widely used in the literature, and has proven to be a robust tool for threshold selection in our own experience.

2.1.3 Isodata Method

Another method for automatic thresholding is the iterative *isodata* method [RC78], which is actually an application of the more general isodata clustering algorithm to the gray values of an image. Like in Otsu's method, the threshold is computed to lie between the means of fore- and background, μ_1 and μ_0, but instead of searching for a global optimum as in (5), the search is performed locally. Given an initial threshold $\theta^{(0)}$, e.g., half of the maximum gray value, the isodata algorithm can be stated as follows:

1. At iteration i, generate binary image $g^{(i)}$ from f using $\theta^{(i)}$.
2. Compute the mean gray values $\mu_0^{(i)}$ and $\mu_1^{(i)}$ of current fore- and background voxels, respectively.
3. Set $\theta^{(i+1)} = (\mu_0^{(i)} + \mu_1^{(i)})/2$, and repeat until convergence.

Similar to the method given in Sec. 2.1.2, the underlying assumption here is that fore- and background gray values can be characterized by different means, μ_0 and μ_1. This method is widely used in $2D$ image processing, particularly in medical applications.

2.1.4 Bayesian Thresholding

From a statistical point of view, thresholding is an easily solvable task if we have a proper image model. In a Bayesian setting, the posterior probability of observing $f(\mathbf{x})$ is simply $p(f(\mathbf{x})|j)$, where $j \in \{0, 1\}$ is the unknown class label, i.e., background and foreground. By Bayes' Theorem we know that

$$p(f(\mathbf{x})|j) \propto p(j)p(j|f(\mathbf{x})). \tag{6}$$

This equation can be applied for determining the global image threshold θ. Assume that the gray values of voxels belonging to fore- and background follow normal distributions about class means $\mu_0 \neq \mu_1$. Furthermore, let us assume that gray value variation in each class is equal, $\sigma_0 = \sigma_1 = \sigma$. Then the likelihood $p(j|f(\mathbf{x}))$ is given by

$$p(j|f(\mathbf{x})) \quad = \quad \frac{1}{\sqrt{2\pi}\sigma} \exp\left(-\frac{(f(\mathbf{x})-\mu_j)^2}{2\sigma^2}\right), \tag{7}$$

where μ_j is the class conditional mean value, as defined in Sec. 2.1.2. The optimal threshold θ can then be found as the gray value of equal log posterior.

$$\begin{aligned} \log p(\theta|0) &= \log p(\theta|1) \\ \log p(0) - \frac{1}{2\sigma^2}(\theta-\mu_0)^2 &= \log p(1) - \frac{1}{2\sigma^2}(\theta-\mu_1)^2 \\ \theta &= \frac{1}{2}(\mu_1+\mu_0) + \frac{\sigma^2}{\mu_0-\mu_1}\log\frac{p(0)}{p(1)} \end{aligned} \tag{8}$$

Eq. (8) gives the optimal threshold for separating two regions which follow Gaussian gray value distributions with equal variance and different means. The restriction of equal variance can also be dropped which results in a slightly more complicated term for the threshold parameter.

An example how this thresholding selection rule was successfully applied is the "Mardia-Hainsworth algorithm", which will be described, below.

Note also that the threshold selection scheme that was described in this section is only one small example of how Bayesian methods can be applied to image processing. The Bayesian framework is the most powerful toolbox for statistical modeling at all stages of image processing, from image denoising, segmentation to object recognition. We will outline the general Bayesian modeling concept in Sec. 5.3, but giving an overview over this wide field is beyond the scope of this review.

2.2 Local Thresholding

Local thresholding can compensate for some shortcomings of the global thresholding approach. As mentioned above, intensity levels of an image can vary depending on the location within a data volume. One common approach for preprocessing in 2D image processing is to calculate the mean intensity value within a window around each pixel and subtract these sliding mean values from each pixel ("shading correction").

In the same spirit, but instead of modifying the image content prior to binarization, one can use a spatially varying threshold, $\theta(\mathbf{x})$, to compensate for these inhomogeneous intensities.

$$g(\mathbf{x}) = \begin{cases} 1 & \text{if } f(\mathbf{x}) \geq \theta(\mathbf{x}) \\ 0 & \text{else} \end{cases} \tag{9}$$

As was the case for the global thresholding approach, (9) does not provide any clues on how these threshold values $\theta(\mathbf{x})$ should be computed. Some common approach to local thresholding will be described, next.

2.2.1 Niblack Thresholding

In [TJ95], Trier and Jain obtained the best results among 11 tested local thresholding algorithms using a method due to Niblack [Nib86]. Niblack's algorithm calculates local mean and standard deviation to obtain a threshold.

$$\theta(\mathbf{x}) = \text{Mean}\left\{f(\mathbf{x}')|\ \|\mathbf{x}-\mathbf{x}'\|_\infty \leq W\right\} + \lambda\sqrt{\text{Var}\left\{f(\mathbf{x}')|\ \|\mathbf{x}-\mathbf{x}'\|_\infty \leq W\right\}} \tag{10}$$

Mean and Var denote the local empirical mean and variance, centered at voxel location $\mathbf{x}$ and using window size W. λ is a parameter of this method. The binarization rule described by (10) implicitly assumes smooth fore- and background areas, where the gray values vary about some unknown mean, which is estimated in a window around the current coordinate $\mathbf{x}$.

Trier and Jain found $W = 15$ and $\lambda = -0.2$ to work best for their 2D application [TJ95]. In 3D, this approach works well in practice when the window size W can be chosen to correspond to the size of objects that are present in the image. The system will fail, on the other hand, in large low–contrast areas:

Assume the current window of size W at $\mathbf{x}$ contains a smooth area with little noise. Then, the estimated variance will be low, resulting in false segmentations caused by noise or lower frequency variations within the image

A heuristic modification of Niblack's formula which solves this problem has been proposed by Sauvola and Pietikäinen [SP00]. Again, a threshold at $\theta(\mathbf{x})$ is computed in a window of size W, but with an additional parameter R.

$$\theta(\mathbf{x}) = \text{Mean}\left\{f(\mathbf{x}')|\ \|\mathbf{x}-\mathbf{x}'\|_\infty \leq W\right\}\left(1+\lambda\left(\frac{\sqrt{\text{Var}\left\{f(\mathbf{x}')|\ \|\mathbf{x}-\mathbf{x}'\|_\infty \leq W\right\}}}{R}-1\right)\right) \tag{11}$$

The newly introduced parameter R can be thought of as an approximate normalization of the standard deviation. In [SP00], it was proposed to set $R = 128$ for 8-bit (unsigned) data, and it turns out in practice that setting R to half the maximal data range is a good choice: The exact value of R is not so crucial as long as the values of $\sqrt{\text{Var}\{\cdot\}}/R$ stay in the range between zero and one for most voxels. For negative λ, this term effectively sets the local threshold close to the mean value in high contrast areas (such as object edges), and above the mean in low–contrast areas (such as large background regions).

As was mentioned above, (11) is a heuristic modification of (10), but it often yields better results in practice.

2.2.2 Mardia and Hainsworth Method

In [MH88], Mardia and Hainsworth proposed an algorithm for spatial thresholding. Their idea was to obtain random variables $G(\mathbf{x})$ at each voxel location $\mathbf{x}$ as linear combinations of the neighboring voxels $\mathbf{x}'$,

$$G(\mathbf{x}) = \sum_{\mathbf{x}'\in N(\mathbf{x})\cup\{\mathbf{x}\}} \gamma_{\mathbf{x}'} F(\mathbf{x}'), \tag{12}$$

where the coefficients γ need to be specified. The authors discuss several possible solutions to the problem of selecting a local threshold $\theta(\mathbf{x})$ being given G and the method they propose to use, described below, is known as the "Mardia–Hainsworth algorithm". As a matter of fact, Eq. (12) was again used later for so-called *kriging* threshold computation by others, see below.

The main observation in [MH88] was that given coefficients γ, one can interpret G as a voxel value and the threshold problem again reduces to voxel–wise thresholding. Thus, the global Bayesian threshold selection method described in Sec. 2.1.4 can be applied to each $G(\mathbf{x})$ to obtain a local thresholding algorithm.

As in Sec. 2.1.4, the underlying assumption to the Mardia–Hainsworth algorithm is that the foreground and background gray values in an image are following normal distributions with parameters (μ_0, σ) and (μ_1, σ), respectively, where it was again assumed that variances are the same. Then, G will also be a Gaussian random variable, with class–conditional mean μ_i^G, $i \in \{0, 1\}$, given by

$$\mu_i^G \quad = \quad \left(\sum_{\mathbf{x}'\in N(\mathbf{x})\cup\{\mathbf{x}\}} \gamma_{\mathbf{x}'}\right)\mu_i. \tag{13}$$

For practical applications, it is recommended in [MH88] to set $\gamma_{\mathbf{x}'} = 1/|N(\mathbf{x}) \cup \{\mathbf{x}\}|$, resulting in a local mean with $\mu_i^G = \mu_i$. The optimal local threshold θ is then given by (8). The complete Mardia–Hainsworth algorithm consists of this local thresholding with a median filter to suppress noisy voxels:

1. For each voxel $\mathbf{x}$, perform thresholding of $G(\mathbf{x})$ using (8) with $\gamma = 1/|N(\mathbf{x}) \cup \{\mathbf{x}\}|$ (local mean).
2. Median filter of the resulting image with mask size $3 \times 3 \times 3$, update μ_0, μ_1, and σ.

These two steps are iterated until convergence. In effect, this is a local Bayesian thresholding operating on voxel values that were smoothed with a mean filter. Note that the cost of computation is significantly higher than for the other methods that have been described, so far.

2.2.3 Indicator Kriging

Thresholding by indicator kriging was described by Oh and Lindquist [OL99]. Kriging is an interpolation method that is commonly used in geostatistics. It relies mainly on local covariance estimates for thresholding and is similar to the Mardia–Hainsworth method in that it estimates the value at voxel $\mathbf{x}$ using a linear combination of its neighbors. Kriging estimators build upon the linear combination $G(\mathbf{x})$ from (12) with $\gamma_{\mathbf{x}} = 0$, i.e., the central voxel is not included in the linear combination. *Indicator* kriging is a modification of this linear combination where the continuous voxel distribution $F(\mathbf{x})$ is replaced by a binary variable i,

$$\begin{aligned} G(\mathbf{x}) &= \sum_{\mathbf{x}' \in N(\mathbf{x})} \gamma_{\mathbf{x}'}\ i(\theta;\ f(\mathbf{x}')) \qquad (14) \\ \text{where} \qquad & i(\theta;\ f(\mathbf{x})) := \begin{cases} 1 & \text{if } f(\mathbf{x}) < \theta \\ 0 & \text{otherwise.} \end{cases} \end{aligned}$$

Note that this definition of i differs from the convention for thresholds, made above, where larger voxel values corresponded to foreground in the image. The quantity of interest is the threshold value θ, and if we knew its density $p(\theta)$, we could compute the optimal threshold. This unknown distribution is approximated by (14) with coefficients γ chosen to minimize the mean square error to the unknown $p(\theta)$. If we require the the coefficients γ to be normalized such that $\sum_{\mathbf{x}'} \gamma_{\mathbf{x}'} = 1$, we can interpret the outcome as the probability of the gray value in voxel $\mathbf{x}$ not exceeding threshold θ:

$$\begin{aligned} p(\theta;\ \mathbf{x}) &= \Pr\left(f(\mathbf{x}) \le \theta\right) \\ &= G(\mathbf{x}) = \sum_{\mathbf{x}' \in N(\mathbf{x})} \gamma_{\mathbf{x}'}\ i\left(\theta;\ f(\mathbf{x}')\right). \qquad (15) \end{aligned}$$

With the normalized coefficients γ, (14) is an unbiased estimator and therefore its mean square error (MSE) is given by

$$\begin{aligned} \text{MSE} &= \text{Var}[p(\theta) - p(\theta;\ \mathbf{x})] = \text{E}[(p(\theta) - p(\theta;\ \mathbf{x}))^2] = \text{E}[(i(\mathbf{x}) - \sum_{\mathbf{x}' \in N(\mathbf{x})} \gamma_{\mathbf{x}'} i(\mathbf{x}'))^2] \\ &= \text{E}\left[\Big(\sum_{\mathbf{x}' \in N(\mathbf{x}) \cup \{\mathbf{x}\}} a_{\mathbf{x}'} i(\mathbf{x}')\Big)^2\right] = \sum_{\mathbf{x}'} \sum_{\mathbf{x}''} a_{\mathbf{x}'} a_{\mathbf{x}''} C_i(\mathbf{x}' - \mathbf{x}''). \qquad (16) \end{aligned}$$

The coefficients a are defined such that $a_{\mathbf{x}} = 1$ and $a_{\mathbf{x}'} = -\gamma_{\mathbf{x}'}$. $C_i(\cdot)$ is the covariance of the indicators. Taking the normalization constraint for coefficients γ and a multiplier λ, minimization of (16) with respect to $\gamma_{\mathbf{x}'}$ (or its substitutes a) can be put as a Lagrangian optimization problem:

$$\begin{aligned} L_\lambda &= \sum_{\mathbf{x}'} \sum_{\mathbf{x}''} a_{\mathbf{x}'} a_{\mathbf{x}''} C_i(\mathbf{x}' - \mathbf{x}'') + \lambda \left(\sum_{\mathbf{x}'} a_{\mathbf{x}'} - 1\right) \\ \frac{dL_\lambda}{da_{\mathbf{x}'}} &= \sum_{\mathbf{x}''} \gamma_{\mathbf{x}''} C_i(\mathbf{x}' - \mathbf{x}'') + \lambda = C_i(\mathbf{x}' - \mathbf{x}). \qquad (17) \end{aligned}$$

Here we made use of the assumption that gray value statistics are stationary in the image. To estimate the indicator covariances in (17), an initial estimate of the image regions must be given. This results in the following algorithm, called *indicator kriging segmentation*:

1. Derive an initial estimate of two thresholds θ_0 and θ_1 from the image histogram, dividing $f(\mathbf{x})$ into disjoint sets of certain foreground and background positions.

2. Estimate the covariance function C_i from indicators i.

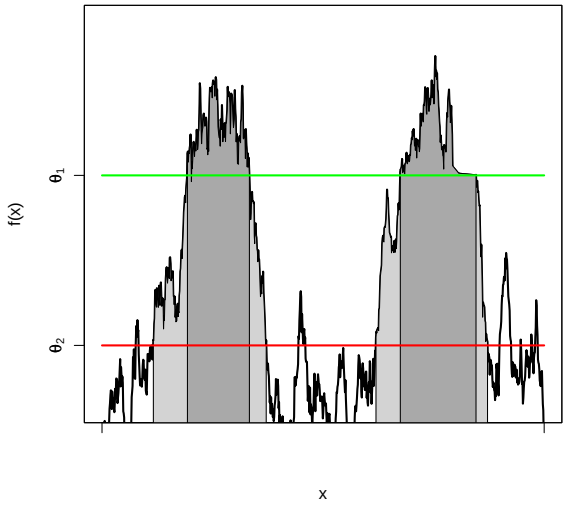

Figure 2: Illustration of hysteresis thresholding: Foreground regions must contain voxels exceeding a "high threshold" but can be extended until reaching a lower threshold. This ensures connected regions and efficiently excludes background noise voxels.

3. Minimize MSE by solving (17), giving the set of coefficients $\{\gamma_{\mathbf{x}'}\}$.

4. If $p(\theta_0;\ \mathbf{x}) > 1 - p(\theta_1;\ \mathbf{x})$, assign $\mathbf{x}$ to background, otherwise to foreground. Return to step 2.

Similar to the Mardia–Hainsworth algorithm shown above, median filtering is used in [OL99] to remove noisy voxels. One main difference of indicator kriging segmentation to that algorithm is that covariance estimates are used.

2.3 Hysteresis

Another common problem in image segmentation is that the segments of interest may well be defined by their intensities, but that there also exist other structures (e.g., noise) with high values. Global thresholding would either underestimate the size of the true segments (because θ was too large) or would include noise in the foreground (because θ was chosen too low).

One way of dealing with such situations where the voxel value distributions of fore- and background voxels overlap is hysteresis thresholding, also known as "double thresholding". It was proposed in [Can86] as a method to segment connected edges from an edge strength map. Hysteresis thresholding uses two thresholds, $\theta_1 > \theta_2$, and starts from voxels $\mathbf{x}$ with $f(\mathbf{x}) \geq \theta_1$. Then all voxels $\mathbf{x}'$ are iteratively assigned to the foreground which are neighbors of an already identified foreground voxel and which fulfill the condition $f(\mathbf{x}') \geq \theta_2$.

This procedure ensures segmentation of connected regions, since a number of "certain" foreground elements are selected while its neighbors may have a lower value. At the same time, noisy background voxels are suppressed by the higher threshold θ_1. See Fig. 2 for an illustration.

Note that this algorithm bears some similarity to the region growing algorithms that will be introduced in Sec. 3. Yet, hysteresis thresholding is more efficiently implemented using *geodesic reconstruction* [Soi99]: Let $\oplus$ denote the *dilation* operator using structuring element W. Dilation enlarges the foreground region of a binary image g by adding voxels to the borders of existing foreground in the directions described by W, see e.g. [Soi99] for details. Using $\wedge$ as the voxel–wise logical *and* operation, geodesic reconstruction is iterative dilation and masking of g:

$$R_m(g) \quad = \quad \big(g \oplus W\big) \wedge m. \tag{18}$$

```
1  funct RegGrow(seed) ≡
2    ⌈
3      region.empty()
4      region.add(seed)
5      while region.HasNeighbour() do
6              x := PopNeighbour(region)
7              if M(x)
8                region.add(x)
9              fi
10     od
11     return(region)
12   ⌋.
```

Figure 3: A generic region growing algorithm: Starting from *seed*, neighboring voxels are added to *region* as long as they fulfill some condition $M(x)$.

Here, m is the so-called mask image. This rule is applied until convergence, i.e., when dilating and "masking" the result with m results in the same image again. Thus, in (18), the dilation is stopped when a region defined by m is exceeded. Hysteresis thresholding is equivalent to a geodesic reconstruction where the marker image m is given by the low-threshold regions, defined by threshold θ_2, and the dilation series is started from the high-threshold (θ_1) seed points.

3 Region Growing

The philosophy behind all region growing algorithms is that all voxels belonging to one object are connected and similar according to some predicate. A generic region growing algorithm is given in Fig. 3. Apart from the choice of an appropriate neighborhood system and the seed selection, the only difference between the numerous region growing methods lies in specifying the predicate M. Some of these will be discussed in this section. We will assume that an appropriate neighborhood system has been chosen for implementing the generic function "PopNeighbour".

Note that in this survey, we view region growing as a voxel-based procedure, where an object is formed from a group of voxels. A different view on region growing is "split&merge". There, an image is initially split into smaller regions, e.g., down to individual voxels. Neighboring regions are then merged if they fulfill a homogeneity criterion like the one used in Algorithm 3. See e.g. [BB82, Ch. 5] for details on this alternative view on region growing methods.

In seeded region growing, seed selection is crucial but can be seen as an external task, often done by hand in medical image processing. Unseeded region growing was also proposed and will be discussed in a later section.

3.1 Growing by Gray Value

One of the more commonly used region growing criteria is based on the observation that an object's gray values are usually within some range around a mean value. Thus, while growing a region, its current mean and standard deviation are computed and a new voxel is added if its value lies within a range around the region's mean.

$$
\begin{aligned}
M(\mathbf{x}) &:= \Big(\mid f(\mathbf{x}) - \mu_R \mid \leq c\sigma_R \Big) \qquad (19)\\
&\text{where}\\
R &:= \{\mathbf{x}' \mid \mathbf{x}' \text{ belongs to region}\}\\
\mu_R &:= \text{Mean}\,\{f(\mathbf{x}) | \mathbf{x} \in R\}\\
\sigma_R &:= \sqrt{\text{Var}\,\{f(\mathbf{x}) | \mathbf{x} \in R\}}
\end{aligned}
$$

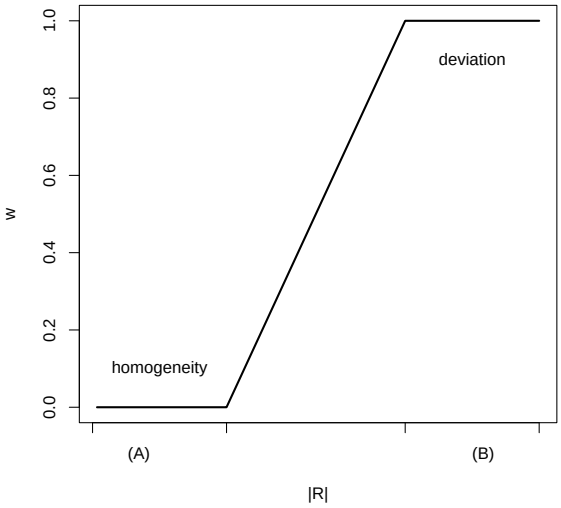

Figure 4: Weighting function for adapting the growing criterion according to the region's size [MPO+97]: (A) Voxels are added to small regions if their local neighborhood is homogeneous, (B) larger regions are grown according to the square deviation from the region's mean.

Except for the region seed, the only parameter of this method is $c \in \mathbb{R}^+$, the coefficient defining the allowed deviation from the region's mean. Since mean and variance can be updated as one voxel after another is added, this region growing algorithm is easily implemented. It can give reasonable segmentation results where objects are connected and can be characterized by their gray values.

3.2 Adaptive Region Growing

A growing criterion called adaptive region growing was proposed in [MPO+97] for segmentation of the human cortex. Their idea was to adapt the decision function according to the region's size: Initially, for a region containing very few voxels, voxels are added as long as a homogeneity (gray value variance) threshold around the region is not exceeded. Then, when a certain number of voxels has been added to the region, one assumes that the gray level statistics of this region have approached the object's true distribution. Thus, further voxels are added only if their gray values are close to the region's mean gray value. Using R, μ_R and σ_R as in (19) and a region size dependant weight w, the adaptive region growing criterion is given by

$$\begin{aligned} M(\mathbf{x}) &:= \left(\frac{1}{T_R} \frac{(f(\mathbf{x}) - \hat{f}_R)^2}{\sigma_R^2} w + \frac{\sigma_N^2}{T_N}(1-w) \leq 1 \right), \qquad (20) \\ \text{where} & \\ \sigma_N &:= \sqrt{\mathrm{Var}\left\{ f(\mathbf{x}) \mid \exists \mathbf{x}' \in N(\mathbf{x}) : \ \mathbf{x}' \in R \right\}}, \\ w &:= w(\mid R \mid) \\ T_R, T_N > 0 & \quad \text{thresholds for enlarging } R. \end{aligned}$$

Small regions will only be enlarged when σ_N^2 does not exceed T_N. For large regions, only voxels for which $(f(\mathbf{x}) - \mu_R)^2/\sigma_R^2$ does not exceed T_R will be added. The weighting function w, depending on the region size $|R|$, determines the point where the cost function switches from homogeneity to gray value difference. Modayur et al. use a linear interpolation between the two terms in (20) as the region's size increases, from zero for small regions (homogeneity only) to one for large regions (gray value deviation only), see Fig. 4.

The authors of [MPO+97] applied this region growing method to neurological images of the human brain. But the idea of adaptive region growing can easily be extended to model other situations, where growing based on gray level difference (for large regions) may not be appropriate. One can generalize the growing criterion from (20) and obtains

$$M(\mathbf{x}) \quad = \quad \big(w\Phi_1(\mathbf{x}) + (1-w)\Phi_0(\mathbf{x}) \leq 1\big). \tag{21}$$

All that is left from the original formulation is the weighting, which still interpolates between two cost terms depending on the region's size. One may use (21), for example, to again start growing a region based on gray value homogeneity (using Φ_0) and then continue to add voxels to match some prior object shape information (using Φ_1)

A similar concept was discussed in [BB82, Sec. 5.5] under the title "semantic region growing". Regions were first merged until they attained a significant size, in this case defined by a ratio of area and perimeter. A Bayesian decision was used for larger regions to determine if two regions should be merged or not.

3.3 Adams Seeded Region Growing

The two region growing methods described above considered one region R at a time. Let us next examine the situation where the image contains m disjoint regions $(R_1, R_2, \ldots, R_m)$. In [AB94], a seeded region growing method was proposed that segments a whole image by picking so-called "boundary voxels" and adding them to regions based on a distance measure. The boundary voxels B are adjacent to at least one region R_i and do not belong to any region in the image.

$$B \quad := \quad \left\{ \mathbf{x} \notin \bigcup_i R_i \mid N(\mathbf{x}) \cap \bigcup_i R_i \neq \emptyset \right\} \tag{22}$$

The algorithm, which originally deals with $2D$ images, picks voxel $\mathbf{x}' \in B$ which has minimal distance δ to any region within the image. The distance measure δ used in [AB94] is the absolute difference of gray value to a region's mean. Thus, pick a voxel $\mathbf{x}'$ with

$$\mathbf{x}' \quad = \quad \text{argmin}_{\mathbf{x}\in B,R}\big(\delta(\mathbf{x}, R)\big), \tag{23}$$

with

$$\delta(\mathbf{x}, R) \quad := \quad |f(\mathbf{x}) - \mu_R| \tag{24}$$

and assign it to the region R_i which minimizes (23). This algorithm is very similar to the ones proposed in the previous sections, in that it selects the voxels that will be added to a region from a local neighborhood. At the same time, it differs from these algorithms since the regions "compete" against each other: Search for a voxel is performed over all regions, not for one region at a time.

3.4 Non-connected Region Growing

A region growing algorithm that can segment non connected regions was proposed by Revol et al. [RJ97] and was also extended to a parameter-free method by using an "assessment function" [RMPCO02], see Sec. 3.5.2.

The unique feature of this algorithm is that voxels may not only be added, but also removed from a region. To achieve this, the so-called "k-contraction" is used. k-contraction removes k voxels from the region, starting from the voxel with the lowest gray value, in increasing order. Note that this procedure assumes that object voxels have larger gray values than background voxels. The procedure is repeated until a homogeneous region is produced, where a region is called homogeneous if its gray value variance is below some threshold $\sigma_{\max}$.

Parameters of this method are the seeds for initialization of the region and the homogeneity parameter $\sigma_{\max}$. The region R is grown until convergence by first applying a dilation, i.e., adding neighboring voxels, and then trimming the region using the k-contraction method described above. Because of

```
1  funct Revol(seed) ≡
2    ⌈
3      n = 1
4      R_0 = {seed}
5      while R_i ≠ R_{i−1} do
6              R_{i+1} = R_i ⊕ W
7              k = 0
8              while (Variance(R_{i+1}) > σ_max) do
9                      k = k + 1
10                     R_{i+1} = k-contraction(R_{i+1})
11             od
12             i = i + 1
13     od
14     return(R_i)
15   ⌋.
```

Figure 5: Non-connected region growing according to [RJ97], where $\oplus$ denotes dilation with structuring element W: Region R_i at iteration i is enlarged by dilation. The result is "contracted" by removing voxels from R_{i+1} until the the gray value variance, $Variance(R_{i+1})$, falls below the parameter $\sigma_{\max}$.

the contraction, which trims the histogram, it is possible for a region to fall apart into non connected components. A pseudo code of this algorithm is given in Fig. 5.

This algorithm differs significantly from the region growing methods described earlier. In this approach, growing and homogeneity testing are separate processes. This way, voxels that were regarded as belonging to an object early in the growing process, may be removed later on. This also means that the value distribution within a region is more flexible during the growing phase. We will describe how Revol et al. extended this algorithm to a parameter-free growing algorithm in Sec. 3.5.2.

3.5 Parameter-Free Region Growing

For all region growing methods described so far, one needs to select seed voxels. Thresholding, as described in Sec. 2, may be used for this initialization step. Here, one should apply thresholding conservatively. By this we mean that the purpose is not to segment the entire object. It is more important to choose a number of certain object voxels, from which to start region growing. In practice, this is often done manually. Region growing methods that do not depend on such initialization have been proposed and we will describe two of these in this section.

3.5.1 Unseeded Region Growing

Lin et al. [LJT01] proposed an implementation of Adams' seeded region growing, presented in Sec. 3.3, which does not need to be initialized by any seed points. However, it is not entirely parameter-free: It requires a threshold θ. This threshold is used to decide if a voxel certainly belongs to a region. Let's describe the algorithm formally. As in Sec. 3.3, the set of unlabeled, region-bordering points (boundary voxels) is defined as

$$B := \left\{ \mathbf{x} \notin \bigcup_i R_i \mid N(\mathbf{x}) \cap \bigcup_i R_i \neq \emptyset \right\}, \tag{25}$$

where

R_i are $1 \ldots \mathrm{m}$ regions in the image.

Initially, the list of regions contains just one region, R_1, which contains just one voxel. This could be any voxel within the dataset. The same distance measure $\delta(\mathbf{x}, R)$ as in Eq. (24) is used, see Sec. 3.3.

Then, if there exists an $\mathbf{x} \in B$ for which $\delta(\mathbf{x}, R_i) \leq \theta$, for some existing region R_i, then $\mathbf{x}$ is added to that region.

If no such voxel was found, it means that there is no boundary voxel that fulfills the similarity constraint. In the following step, the voxel $\mathbf{x}$ is searched which has the smallest distance δ among all voxels and all existing regions,

$$(\mathbf{x}^*, R^*) \quad = \quad \text{argmin}_{(\mathbf{x}', R')}\{\delta(\mathbf{x}', R')\}. \tag{26}$$

The obtained voxel $\mathbf{x}^*$ is not adjacent to region R^*, otherwise we would have found it in the first step. Now, if $\delta(\mathbf{x}^*, R^*) \leq \theta$, we can add $\mathbf{x}^*$ to R^*. If not, then there exists no region which is similar enough to $f(\mathbf{x}^*)$. Therefore, create a new region R_{m+1}, containing the voxel $\mathbf{x}^*$, and restart the whole procedure.

Thus, the number of regions in the image increases. The authors of [LJT01] note that the solution thus found may not be the optimal one because a voxel may not be added to the region which it most closely resembles if that region is created after the voxel was visited. They propose to re-evaluate the neighborhood of any newly created region to lessen this effect.

The nice feature of Lin et al.'s algorithm is that the scheme is not limited to Adams' value distance criterion. In fact, we may substitute a measure that is more appropriate for a given application and apply their scheme for unseeded region growing. We are not aware of any work where this was done.

3.5.2 Assessment Function

This section expands on the region growing algorithm by Revol et al. described in Sec. 3.4. The idea described in [RMPCO02] is to design an assessment function depending on an algorithm's parameters, in this case $\sigma_{\max}$, and then to optimize this functional over a given parameter range. Thus, this is a more general parameter estimation approach which may also be applied to other methods.

Firstly, Revol at al. propose using Otsu's thresholding algorithm followed by an erosion to initialize the seeds of their algorithm, c.f. Sec 2.1.2. For the homogeneity parameter σ, an assessment function $f_a(\sigma)$ is designed, with respect to which an optimal homogeneity parameter is estimated as

$$\sigma_{\max} \quad = \quad \max_{\sigma'}\big(f_a(\sigma')\big). \tag{27}$$

Revol et al. propose and evaluate six different assessment functions, two of which we will discuss here. As noted above, this method for choosing an algorithm's parameters is quite general and an appropriate assessment function should be chosen depending on the application. In [RMPCO02], two types of assessment functions were discussed: boundary and region assessment functions.

Using a boundary assessment function implicitly says that a region can be well defined by its edges. This is true in many imaging situations. It was proposed to use a functional of the form

$$f^{\text{boundary}}(\sigma) \quad = \quad \frac{1}{\mid B(R) \mid} \sum_{\mathbf{x} \in B(R)} \sum_{\mathbf{x}' \in N(\mathbf{x}) \wedge \mathbf{x}' \notin R} \mid f(\mathbf{x}) - f(\mathbf{x}') \mid, \tag{28}$$

where

$R = R(\sigma)$ is the algorithm′s result using homogeneity threshold σ,

$B(R)$ is the boundary of R, defined as all but the interior of R.

Eq. (28) will choose the homogeneity threshold σ_{max} for the algorithm in Fig. 5 which will have the largest average contrast along the region's border. In other words, the parameter $\sigma_{\max}$ which best fits regions to image edges is chosen.

A "region-based" assessment function was given as

$$f^{\text{region}}(\sigma) = \left(\sqrt{\sum_{\mathbf{x}\in R} \left(f(\mathbf{x}) - \mu_R\right)^2 + \sum_{\mathbf{x}\in R^C} \left(f(\mathbf{x}) - \mu_{R^C}\right)^2} \right)^{-1}, \tag{29}$$

where

$R = R(\sigma)$ is the algorithm′s result using homogeneity threshold σ,

$R^C = \{\mathbf{x} \mid \mathbf{x} \notin R\}$,

$\mu_R = \text{Mean}\left[f(\mathbf{x})\right] \ \forall \mathbf{x} \in R$

$\mu_{R^C} = \text{Mean}\left[f(\mathbf{x})\right] \ \forall \mathbf{x} \notin R.$

This assessment function implicitly enforces regions which closely resemble the underlying image's values. Note that this is very similar to the segmentation cost function proposed by Mumford and Shah, which we discuss in Sec. 5.4, except that here no penalization term for long region boundaries is used.

Revol et al. tested these two and further assessment functions on a two-dimensional image containing a regular grid of lines, which represents one connected region. The number of common voxels in the segmentation and ground truth were counted and normalized by the number of true and found points. This gave an error measure equal to one for a perfect segmentation and less than one otherwise.

The two assessment functions that we presented in this section gave similar results and were among the best-performing assessment functions in that paper. The method was tested on 3D MIR and synchrotron radiation CT images of human calcaneus bone.

4 Deformable Surfaces and Level Set Methods

This section deals with some model-based approaches to image segmentation that have widely been applied in 2D and 3D medical image processing.

4.1 Deformable Surfaces

In 2D image segmentation, active contours, also known as "snakes", are parametric curves which one tries to fit to an image, usually to the edges within an image. The original model is due to Kaas et al. [KWT88], but many modifications have been proposed in the literature. Let $\mathcal{C} : [0,1] \rightarrow \Omega_2$ denote a curve in the 2D image domain Ω_2. The original energy functional is then given by

$$E(\mathcal{C}) = \underbrace{\alpha \int_0^1 |\mathcal{C}'(q)|^2 dq + \beta \int_0^1 |\mathcal{C}''(q)|^2 dq}_{E_{\text{int}}} \underbrace{- \lambda \int_0^1 |\bigtriangledown f\left(\mathcal{C}(q)\right)| dq}_{E_{\text{ext}}} \tag{30}$$

The internal energy, E_{int}, is meant to enforce smoothness of the curve, whereas the external energy, E_{ext} pulls the contour towards object edges. Differently speaking, the active contour model is a regularized gradient edge detector.

One much discussed point on snakes is their inability to move into concavities of an object's boundary and their inability to find the borders when it is initialized too far distant from the actual border location. Many researchers have proposed possible solutions to this problem, e.g., gradient vector fields [XP98]. Furthermore, the model in (30) cannot change topology: A curve must always stay closed and is implicitly not allowed to cross. This is dealt with in the level set framework, discussed below.

But before proceeding to level set methods, we need to generalize the 2D active contour model in (30) into a 3D *deformable surface*. The extension of the curve $\mathcal{C}$ to 3D is the parametric surface $\mathcal{S} : [0,1] \times [0,1] \rightarrow \Omega$. Similar to (30), an energy term of external (image) forces and internal (smoothness) constraints is constructed using first and second order derivatives [CKSS97],

$$E(\mathcal{S}) = \int_0^1 \int_0^1 \left(\alpha_r \left| \frac{\partial \mathcal{C}}{\partial r} \right|^2 + \alpha_s \left| \frac{\partial \mathcal{C}}{\partial s} \right|^2 + \beta_{rs} \left| \frac{\partial^2 \mathcal{C}}{\partial r \partial s} \right|^2 + \beta_{rr} \left| \frac{\partial^2 \mathcal{C}}{\partial^2 r} \right|^2 + \beta_{ss} \left| \frac{\partial^2 \mathcal{C}}{\partial^2 s} \right|^2 - \lambda | \bigtriangledown f\left(\mathcal{S}(r,s)\right) | \right) dr ds. \tag{31}$$

$E(\mathcal{S})$ has more parameters than the corresponding energy of the 2D active contour model. Nevertheless, it uses the same principles and is a direct extension to 3D image segmentation.

4.2 Level Sets

Level sets [Set99] implicitly define lower dimensional structures such as surfaces via a function $\Phi : \Omega \rightarrow \mathbb{R}$.

$$\Phi(\mathbf{x}) = c, \tag{32}$$

for some constant c, usually fixed to zero. In other words, a level set is nothing but an iso-surface of the function Φ. What is interesting about this definition is that Φ *implicitly* defines a hyper-surface $\mathcal{S}$ enclosing an image region: Let $R := \{\mathbf{x}|\Phi(\mathbf{x}) < 0\}$, then

$$\mathcal{S} := \partial R, \tag{33}$$

i.e., the boundary of region R is a surface $\mathcal{S}$. Therefore, when looking for a segmentation, given by $\mathcal{S}$, we modify Φ, which implies a modification of the segmentation, rather than modifying $\mathcal{S}$ itself (which was the approach taken by deformable surfaces, see Sec. 4.1). This modification of Φ can influence the shape of $\mathcal{S}$ in many ways, and can also change its topology: In contrast to the definition of $\mathcal{S}$ for the deformable surface model in Sec. 4.1, $\mathcal{S}$ can now break up into disjoint surfaces. Level set methods are based on a partial differential equation and can be solved using finite difference methods. The basic equation underlying level set methods is the *level set equation*, which describes the change of Φ over time (or iteration) t,

$$\Phi_t + \mathbf{V} \cdot \bigtriangledown \Phi = 0. \tag{34}$$

Φ_t is the temporal partial derivative of the level set function, $\bigtriangledown$ denotes the spatial gradient operator and $\mathbf{V}$ describes an external force field guiding the evolution of the curve in the image. This equation is also known in physics, where it is used to represent the reaction surface of an evolving flame.

In image processing, level set methods can for example be applied by defining the external force $\mathbf{V}$ as the gradient field of an image. We are then looking for a steady state solution of Eq. (34), where the surface $\mathcal{S}$ has locked onto object edges. This idea seems very similar to the deformable surface approach, and a level set method that implements deformable surfaces – but without the drawback of fixed topology – will be described in the following section.

4.3 Implicit Deformable Surfaces

The active contours of Witkin and the level set method were combined by Caselles et al. [CKS97], what they called *geodesic active contours*. Their result has proven to be very useful because it combines the intuitive active contours concepts with efficient implementations of level set methods. Additionally, geodesic active contours have the advantage that they can change topology during evolution.

The 3D analog to geodesic active contours, the evolution of an implicit surface $\mathcal{S}$ by modification of a level set function Φ, was described in [CKSS97]. The derivation therein is based on the concept of minimal surfaces: It is observed that finding $\mathcal{S}$ can be put as finding a surface of minimal weighted area, with the weight being given by a function $h(f)$ of the image f. Minimization of this area via the calculus of variations leads to a gradient descent rule in image space, see [CKSS97]. They then show that this minimization procedure can equivalently be implemented by finding the steady state solution, i.e., $\Phi_t = 0$, of the following partial differential equation:

$$\begin{aligned} \Phi_t &= h(f)\,|\bigtriangledown\Phi|\left(\mathrm{div}\frac{\bigtriangledown\Phi}{|\bigtriangledown\Phi|} + \nu\right) + \bigtriangledown h \cdot \bigtriangledown\Phi \qquad (35) \\ \text{where} & \\ h(f) &= \frac{1}{1 + |\bigtriangledown G_\sigma * f|^2}, \\ \mathrm{div}\ \mathbf{v} &= \frac{\partial v_1}{\partial x} + \frac{\partial v_2}{\partial y} + \frac{\partial v_3}{\partial z} \text{ with } \mathbf{v} := \frac{\bigtriangledown\Phi}{|\bigtriangledown\Phi|}. \end{aligned}$$

Here $\bigtriangledown G_\sigma$ denotes the difference of Gaussian (DoG) filter with size σ, and the parameter $\nu > 0$ is a constant force in the normal direction to the level sets of Φ. Eq. (35) is not quite intuitive, but should rather be seen as an appropriate tool for finding a surface $\mathcal{S}$ minimizing (31). That is, by evolving a function Φ until $\Phi_t = 0$ using (35) from some initial estimate Φ_0, one can find a regularized surface $\mathcal{S}$ which is located on edges in the image f.

5 Other Segmentation Concepts

The segmentation methods that were described so far fell into three groups: They were gray–value based (Sec. 2), region based (Sec. 3), or shape based (Sec. 4). What will be described in this section does not fall cleanly into any of these three categories.

5.1 Fuzzy Connectedness

The idea behind fuzzy connectedness is to represent knowledge on the connectedness of voxels by a fuzzy relation [US96]. A fuzzy relation

$$\mu : \Omega \times \Omega \to [0, 1] \tag{36}$$

can be interpreted as a measure of similarity between two voxels. From the point of view of image segmentation, the use of the fuzzy connectedness method lies in finding the connectedness of two voxels $\mathbf{x}, \mathbf{x}' \in \Omega$ and deciding on whether these two voxels belong to the same object or not.

Udupa and Samarasekera use an idea very similar to the principle of bilateral filters (see [TM98]): Whether two voxels $\mathbf{x}$ and $\mathbf{x}'$ within an image belong to the same object depends on their distance $\|\mathbf{x} - \mathbf{x}'\|$ and similarity $|f(\mathbf{x}) - f(\mathbf{x}')|$. They call these two concepts adjacency and affinity, respectively, and define a set of two fuzzy relations: The fuzzy adjacency, μ_ω, and the fuzzy affinity, μ_ξ. In their simplest variant, they take the form of decaying functions of distance, steered by two scalar parameters k_1 and k_2. Two possible definitions for adjacency ω and affinity ξ, taken from [US96] are:

$$\begin{aligned} \mu_\omega(\mathbf{x}, \mathbf{x}') &:= \begin{cases} \frac{1}{1+k_1\|\mathbf{x}-\mathbf{x}'\|} & \text{if } \|\mathbf{x} - \mathbf{x}'\| \le d_{\max} \\ 0 & \text{else} \end{cases} \\ \mu_\xi(\mathbf{x}, \mathbf{x}') &:= \frac{\mu_\omega(\mathbf{x}, \mathbf{x}')}{1 + k_2|f(\mathbf{x}) - f(\mathbf{x}')|}. \end{aligned} \tag{37}$$

Fig. 6 illustrates the dependencies of affinity and adjacency for a simple one–dimensional example. Now that we have defined the affinity between two voxels, we can proceed to defining *fuzzy connectedness*: A path $p_{\mathbf{x}\mathbf{x}'} = (\mathbf{x}, \mathbf{x}_0, \mathbf{x}_1, ..., \mathbf{x}')$ is a sequence of neighboring voxels leading from voxel $\mathbf{x}$ to $\mathbf{x}'$. Denote by $\mathcal{P}_{\mathbf{x}\mathbf{x}'}$ the set of all such valid paths between two points. Each path $p_{\mathbf{x}\mathbf{x}'} \in \mathcal{P}_{\mathbf{x}\mathbf{x}'}$ will contain a "weakest link" in terms of its fuzzy affinity μ_ξ. The connectedness, μ_K, of two voxels can then be defined as as the strongest path in terms of the weakest link's affinity.

$$\mu_K(\mathbf{x}, \mathbf{x}') = \max_{p_{\mathbf{x}\mathbf{x}'} \in \mathcal{P}_{\mathbf{x}\mathbf{x}'}} \left\{ \min_{(\mathbf{x}_i, \mathbf{x}_{i+1}) \in p_{\mathbf{x}\mathbf{x}'}} \left\{ \mu_\xi(\mathbf{x}_i, \mathbf{x}_{i+1}) \right\} \right\} \tag{38}$$

In [US96] and [NFU03], algorithms for computing the fuzzy connectedness between any two points in the image domain are proposed. Within the fuzzy connectedness framework, segmentation of an image reduces to thresholding of the fuzzy connectedness values. Therefore, any two voxels with μ_K exceeding this threshold will be labeled as belonging to one image segment.

5.2 Watershed Algorithm

The watershed transform can be explained very intuitively by an analogy of water filling catchment basins [Soi99]. Firstly, the image is interpreted as a topographic map. Thus, the value in each voxel describes a height at that point (this is easier to imagine in 2D). Now, consider a drop of water falling on

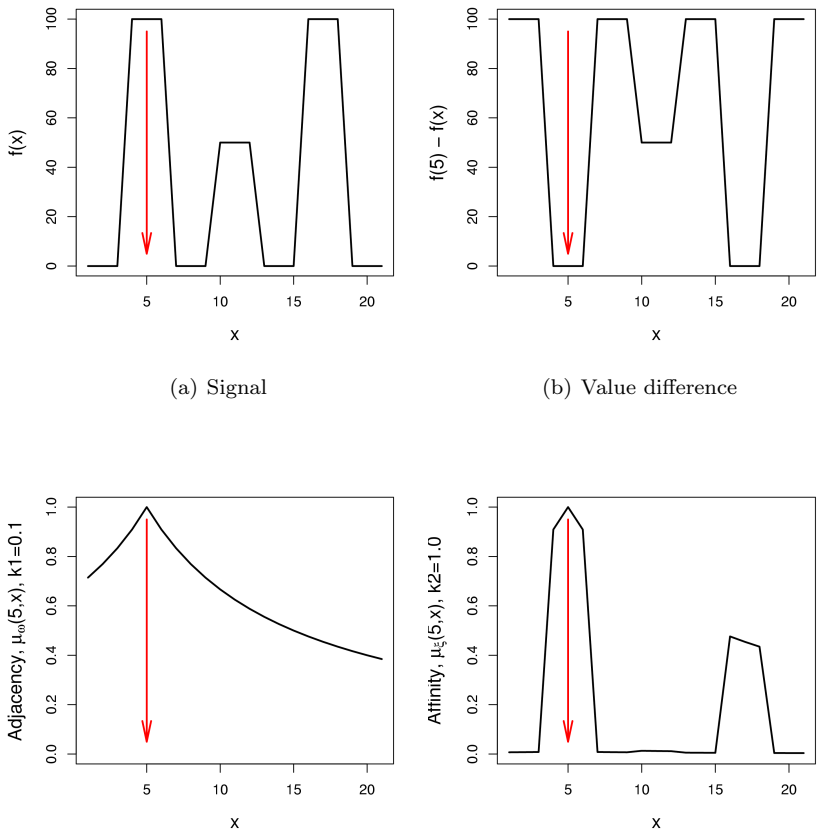

(a) Signal

(b) Value difference

(c) Adjacency

(d) Affinity

Figure 6: Illustration of fuzzy affinity in the 1D case, the reference location $x_0 = 5$ is marked. The adjacency in (c) is a decaying function of distance, whereas the affinity in (d) has local maxima at the reference position and at positions with similar values.

the image. It will follow the path of steepest descent and will be caught in one voxel. Thus, a catchment basin is defined as the set of all voxels from which the path of steepest descent ends in the same voxel.

The watershed algorithm can be implemented by sorting all voxels in the order of increasing value. One starts at the lowest value, assigns a label to all voxels at this level and goes through the list of sorted voxels in increasing order. During this procedure, one has to label voxels according to their neighborhood: If at a value level, a voxel has an already labeled neighbor, it belongs to the same catchment basin. If at one value, a voxel should be assigned more than just one label, it means that at this voxel, one should build a "dam", or watershed, separating two catchment basins. While going upwards through the value list, new, isolated local minima in the topographic map will introduce new labels.

This algorithm could, for example, be used on the gradient strengths to achieve a segmentation using edge information. Watersheds tend to oversegment, and strategies for avoiding this need to be considered. Morphological reconstructions for preprocessing the set of starting points has shown to work well, see [Vin93] for details. A feature of the watershed segmentation is that it will always achieve closed contours since all value levels will be considered by the algorithm.

5.3 Bayesian Methods

Bayesian approaches to image processing treat all involved quantities as random variables and rely on the laws of probability to derive probabilistic models for images. Among the tools of probability, *Bayesian*

decision theory [DH73] is a quite powerful one. In Bayesian decision theory, costs are assigned to each correct or wrong decision, and based on the probabilities of occurring events, the decision that minimizes the *risk* is taken. The risk in Bayesian decision theory is the cost times the probability of a wrong action being taken.

But by far the most important Bayesian approach to image processing are *Markov Random Fields* (MRF), a multidimensional extension of Markov chains. A k–Markov chain is a sequence of random variables, $(X_1, X_2, \ldots, X_n)$, where the marginal density of any one random variable X_i depends only on the k preceding $X_{i-k}, \ldots, X_{i-1}$. Similarly in an MRF, the marginal of random variable X depends not on all other image points, but only on those in some neighborhood. The central result with regard to MRFs is the *Hammersley–Clifford theorem* [GG84], which uniquely characterizes MRFs by Gibbs distributions: $\mathbf{X}$ is a Markov random field if and only if

$$p(\mathbf{x}) = \frac{1}{Z} \exp\big(-\beta \sum_{c \in \mathcal{C}} U(c)\big), \tag{39}$$

where $\mathcal{C}$ denotes the set of all cliques, i.e., mutually neighboring voxels in $\mathbf{X}$, and U is the energy function that describes the interactions between voxels in the MRF $\mathbf{X}$. The immediate implication of the Hammersley–Clifford theorem is that computation of the joint density of all voxels in an image can be reduced to considering local interactions within the cliques $c \in \mathcal{C}$, only.

For an example where MRFs have been applied to 3D image segmentation, see [HKK+97], where the parameters of an MRF model were computed from some manually labeled training samples and the image was segmented using a simulated annealing algorithm.

5.4 Mumford and Shah's Cost Function

The energy function for image segmentation proposed by Mumford and Shah [MS89] has been widely used and its mathematical properties are well analyzed [Cha01]. It is a general approach to image segmentation, where it is assumed that objects can be characterized by smooth surfaces, or volumes in three dimensions. In this section, we deviate from the conventions made in the beginning of this review. In the view of Mumford and Shah, a segmentation does not need to be discrete. In this section, we use $g(\mathbf{x}) \in \mathbb{R}$. Define a set of discontinuities, $K \subset \Omega$, defining the boundaries of the objects.

$$\begin{aligned} E(g, K) &= c_1 \int_\Omega \|g(\mathbf{x}) - f(\mathbf{x})\|^2 d\mathbf{x} + c_2 \int_{\Omega \setminus K} \|\nabla g(\mathbf{x})\|^2 + c_3 l(K) \\ &\text{where} \\ c_1, c_2, c_3 &> 0 \\ l(K) &\quad \text{length of } K \end{aligned} \tag{40}$$

The first term in (40) encourages segmentations g that are an approximation of the original image. Without the other two regularizing terms, an optimal segmentation would simply be the original image. The second term penalizes variation within each component, thus enforcing smooth areas in the segmentation result. This integral leaves out the object boundaries. Thus we only allow discontinuities in the segmentation result at object boundaries. The length of the boundaries between regions needs to be penalized to avoid oversegmentation (for example, simply divide the image into a large number of small homogeneous cubes). Segmentations which minimize (40) will contain homogeneous regions with the mean value of the corresponding regions from the original image.

Implementations of (40) will require optimization routines that fit the segmentation border K to a given image.

6 Conclusions

Even though image segmentation has been a field of active research for many decades (the works cited in this report spread from the 1970's until 2003), it remains to be one of the hardest and at the same time most frequently required steps in image processing systems. Therefore, there does not and can not exist a standard segmentation method that can be expected to work equally well for all tasks. When approaching

a new image processing problem, it is essential to carefully evaluate different available methods and to choose the one that best solves the given task.

Of course, the listing in this report is by no means complete. Some important active research topics such as graph cuts for image segmentation, see [SM00], or the wide field of machine learning applied to image segmentation have not been covered.

Then, why is image segmentation such a hard problem? One possible answer can be given by looking at the definition of a well posed problem in mathematics. A problem is well posed if its solution (1) exists, (2) is unique, and (3) depends continuously on the data. Looking at the image segmentation problem, we may hope for the existence of a solution. But the remaining two criteria will not usually be fulfilled by a segmentation problem, which may explain why we should not expect an almighty image segmentation algorithm to by published anytime soon.

In the meantime, one should resort to the methods that are available, some of which we have just described. A big problem in 3D image processing is the amount of data. Some ideas and concepts that we have described, like region growing, are quite intuitive; but implementing an efficient region growing algorithm that allows one to comfortably deal with datasets of a few hundred megabytes can be a demanding task. Another difficulty when dealing with 3D data are interactivity and visualization: For 2D images, hand–labeling of image points and visual validation of a segmentation result can be done. But 2D projections of 3D data can often give a wrong spatial impression. Therefore it is important to carefully examine segmentation results, not to rely on verification in single slices, and if possible to compare the outcome quantitatively using measurements of some known parameters.

References

[AB94] R. Adams and L. Bischof. Seeded region growing. *IEEE Trans. Pattern Analysis Machine Intelligence*, 16(6):641–647, Jun 1994.

[BB82] D.H. Ballard and C.M. Brown. *Computer Vision*. Prentice-Hall, 1982.

[Can86] J. Canny. A computational approach to edge detection. *IEEE Trans. Pattern Analysis Machine Intelligence*, PAMI-8(6):679–698, Nov 1986.

[Cha01] A. Chambolle. Inverse problems in image processing and image segmentation. In C.E. Chidume, editor, *ICTP Lecture Notes*, volume 2, pages 1–94. ICTP, 2001.

[CKS97] V. Caselles, R. Kimmel, and G. Sapiro. Geodesic active contours. *Int. J. Computer Vision*, 22(1):61–79, 1997.

[CKSS97] V. Caselles, R. Kimmel, G. Sapiro, and C. Sbert. Minimal surfaces based object segmentation. *IEEE Trans. Pattern Analysis and Machine Intelligence*, 19(4):394–398, Apr 1997.

[DH73] R.O. Duda and P.E. Hart. *Patten classification and scene analysis*. Wiley–Interscience, 1973.

[GG84] S. Geman and D. Geman. Stochastic relaxation, gibbs distributions, and the bayesian restoration of images. *IEEE Trans. Pattern Analysis Machine Intelligence*, PAMI-6(6):721–741, Nov 1984.

[HKK+97] K. Held, E.R. Kops, B.J. Krause, W.M. Wells, R. Kikinis, and H.W. Muller-Gartner. Markov random field segmentation of brain MR images. *IEEE Trans. Medical Imaging*, 16(6):878–886, Dec 1997.

[KWT88] M. Kaas, A. Witkin, and D. Terzopoulos. Snakes: Active contour models. *International Journal of Computer Vision*, 1:321 – 331, 1988.

[LJT01] Z. Lin, J. Jin, and H. Talbot. Unseeded region growing for 3D image segmentation. In Peter Eades and Jesse Jin, editors, *Selected papers from Pan-Sydney Workshop on Visual Information Processing*, Sydney, Australia, 2001. ACS.

[MH88] K.V. Mardia and T.J. Hainsworth. A spatial thresholding method for image segmentation. *IEEE Trans. Pattern Analysis Machine Intelligence*, 10(6):919–927, Nov 1988.

[MPO+97] B. Modayur, J. Prothero, G. Ojemann, K. Maravilla, and J. Brinkley. Visualization-based mapping of language function in the brain. *Neuroimage*, 6:245–258, 1997.

[MS89] D. Mumford and J. Shah. Optimal approximations by piecewise smooth functions and associated variational problems. *Communications on Pure and Applied Mathematics*, 42:577–685, 1989.

[NFU03] L.G. Nyúl, A.X. Falcão, and J.K. Udupa. Fuzzy–connected 3D image segmentation at interactive speeds. *Graphical Models*, 64:259–281, 2003.

[Nib86] W. Niblack. *An Introduction to Digital Image Processing*. Prentice Hall, 1986.

[OL99] W. Oh and B. Lindquist. Image thresholding by indicator kriging. *IEEE Trans. Pattern Analysis Machine Intelligence*, 21(7):590–602, Jul 1999.

[Ots79] N. Otsu. A threshold selection method from grey-level histograms. *IEEE Trans. Systems, Man, and Cybernetics*, 9(1):62–66, Jan 1979.

[PP93] N.R. Pal and S.K. Pal. A review on image segmentation techniques. *Pattern Recognition*, 26(9):1277 – 1294, 1993.

[PXP00] D.L. Pham, C. Xu, and J.L. Prince. Current methods in medical image segmentation. *Annual Review of Biomedical Engineering*, 2:315–337, 2000.

[RC78] T.W. Ridler and S. Calvard. Picture thresholding using an iterative selection method. *IEEE Trans. Systems, Man and Cybernetics*, 8(8):630–632, Aug 1978.

[RJ97] C. Revol and M. Jourlin. A new minimum variance region growing algorithm for image segmentation. *Pattern Recognition Letters*, 18:249–258, 1997.

[RMPCO02] C. Revol-Muller, F. Peyrin, Y. Carrillon, and C. Odet. Automated 3d region growing algorithm based on an assessment function. *Pattern Recognition Letters*, 23(1-3):137–150, 2002.

[Set99] J.A. Sethian. *Level Set Methods and Fast Marching Methods*. Cambridge University Press, 2nd edition, 1999.

[SM00] J. Shi and J. Malik. Normalized cuts and image segmentation. *IEEE Trans. Pattern Analysis Machine Intelligence*, 22(8):888–905, Aug 2000.

[Soi99] P. Soille. *Morphological image analysis*. Springer-Verlag, 1999.

[SP00] J. Sauvola and M. Pietikäinen. Adaptive document image binarization. *Pattern Recognition*, 33:225–236, 2000.

[TJ95] O.D. Trier and A.K. Jain. Goal-directed evaluation of binarization methods. *IEEE Trans. Pattern Analysis Machine Intelligence*, 17(12):1191–1201, Dec 1995.

[TM98] C. Tomasi and R. Manduchi. Bilateral filtering for gray and color images. In *Proc. Sixth Int. Conf. Computer Vision (ICCV)*. IEEE Computer Society, 1998.

[US96] J.K. Udupa and S. Samaresekera. Fuzzy connectedness and object definition: Theory, algorithms and applications in image segmentation. *Graphical Models and Image Processing*, 58(3):246–261, 1996.

[Vin93] L. Vincent. Morphological grayscale reconstruction in image analysis: applications and efficient algorithms. *IEEE Trans. Image Processing*, 2(2):176–201, Apr 1993.

[XP98] C. Xu and J.L. Prince. Snakes, shapes and gradient vector flow. *IEEE Trans. Image Processing*, 7(3):359–369, Mar 1998.

Published reports of the Fraunhofer ITWM

The PDF-files of the following reports are available under:
www.itwm.fraunhofer.de/de/zentral__berichte/berichte

1. D. Hietel, K. Steiner, J. Struckmeier
A Finite - Volume Particle Method for Compressible Flows
(19 pages, 1998)

2. M. Feldmann, S. Seibold
Damage Diagnosis of Rotors: Application of Hilbert Transform and Multi-Hypothesis Testing
Keywords: Hilbert transform, damage diagnosis, Kalman filtering, non-linear dynamics
(23 pages, 1998)

3. Y. Ben-Haim, S. Seibold
Robust Reliability of Diagnostic Multi-Hypothesis Algorithms: Application to Rotating Machinery
Keywords: Robust reliability, convex models, Kalman filtering, multi-hypothesis diagnosis, rotating machinery, crack diagnosis
(24 pages, 1998)

4. F.-Th. Lentes, N. Siedow
Three-dimensional Radiative Heat Transfer in Glass Cooling Processes
(23 pages, 1998)

5. A. Klar, R. Wegener
A hierarchy of models for multilane vehicular traffic
Part I: Modeling
(23 pages, 1998)

Part II: Numerical and stochastic investigations
(17 pages, 1998)

6. A. Klar, N. Siedow
Boundary Layers and Domain Decomposition for Radiative Heat Transfer and Diffusion Equations: Applications to Glass Manufacturing Processes
(24 pages, 1998)

7. I. Choquet
Heterogeneous catalysis modelling and numerical simulation in rarified gas flows Part I: Coverage locally at equilibrium
(24 pages, 1998)

8. J. Ohser, B. Steinbach, C. Lang
Efficient Texture Analysis of Binary Images
(17 pages, 1998)

9. J. Orlik
Homogenization for viscoelasticity of the integral type with aging and shrinkage
(20 pages, 1998)

10. J. Mohring
Helmholtz Resonators with Large Aperture
(21 pages, 1998)

11. H. W. Hamacher, A. Schöbel
On Center Cycles in Grid Graphs
(15 pages, 1998)

12. H. W. Hamacher, K.-H. Küfer
Inverse radiation therapy planning - a multiple objective optimisation approach
(14 pages, 1999)

13. C. Lang, J. Ohser, R. Hilfer
On the Analysis of Spatial Binary Images
(20 pages, 1999)

14. M. Junk
On the Construction of Discrete Equilibrium Distributions for Kinetic Schemes
(24 pages, 1999)

15. M. Junk, S. V. Raghurame Rao
A new discrete velocity method for Navier-Stokes equations
(20 pages, 1999)

16. H. Neunzert
Mathematics as a Key to Key Technologies
(39 pages (4 PDF-Files), 1999)

17. J. Ohser, K. Sandau
Considerations about the Estimation of the Size Distribution in Wicksell's Corpuscle Problem
(18 pages, 1999)

18. E. Carrizosa, H. W. Hamacher, R. Klein, S. Nickel
Solving nonconvex planar location problems by finite dominating sets
Keywords: Continuous Location, Polyhedral Gauges, Finite Dominating Sets, Approximation, Sandwich Algorithm, Greedy Algorithm
(19 pages, 2000)

19. A. Becker
A Review on Image Distortion Measures
Keywords: Distortion measure, human visual system
(26 pages, 2000)

20. H. W. Hamacher, M. Labbé, S. Nickel, T. Sonneborn
Polyhedral Properties of the Uncapacitated Multiple Allocation Hub Location Problem
Keywords: integer programming, hub location, facility location, valid inequalities, facets, branch and cut
(21 pages, 2000)

21. H. W. Hamacher, A. Schöbel
Design of Zone Tariff Systems in Public Transportation
(30 pages, 2001)

22. D. Hietel, M. Junk, R. Keck, D. Teleaga
The Finite-Volume-Particle Method for Conservation Laws
(16 pages, 2001)

23. T. Bender, H. Hennes, J. Kalcsics, M. T. Melo, S. Nickel
Location Software and Interface with GIS and Supply Chain Management
Keywords: facility location, software development, geographical information systems, supply chain management
(48 pages, 2001)

24. H. W. Hamacher, S. A. Tjandra
Mathematical Modelling of Evacuation Problems: A State of Art
(44 pages, 2001)

25. J. Kuhnert, S. Tiwari
Grid free method for solving the Poisson equation
Keywords: Poisson equation, Least squares method, Grid free method
(19 pages, 2001)

26. T. Götz, H. Rave, D. Reinel-Bitzer, K. Steiner, H. Tiemeier
Simulation of the fiber spinning process
Keywords: Melt spinning, fiber model, Lattice Boltzmann, CFD
(19 pages, 2001)

27. A. Zemitis
On interaction of a liquid film with an obstacle
Keywords: impinging jets, liquid film, models, numerical solution, shape
(22 pages, 2001)

28. I. Ginzburg, K. Steiner
Free surface lattice-Boltzmann method to model the filling of expanding cavities by Bingham Fluids
Keywords: Generalized LBE, free-surface phenomena, interface boundary conditions, filling processes, Bingham viscoplastic model, regularized models
(22 pages, 2001)

29. H. Neunzert
»Denn nichts ist für den Menschen als Menschen etwas wert, was er nicht mit Leidenschaft tun kann«
Vortrag anlässlich der Verleihung des Akademiepreises des Landes Rheinland-Pfalz am 21.11.2001
Keywords: Lehre, Forschung, angewandte Mathematik, Mehrskalenanalyse, Strömungsmechanik
(18 pages, 2001)

30. J. Kuhnert, S. Tiwari
Finite pointset method based on the projection method for simulations of the incompressible Navier-Stokes equations
Keywords: Incompressible Navier-Stokes equations, Meshfree method, Projection method, Particle scheme, Least squares approximation
AMS subject classification: 76D05, 76M28
(25 pages, 2001)

31. R. Korn, M. Krekel
Optimal Portfolios with Fixed Consumption or Income Streams
Keywords: Portfolio optimisation, stochastic control, HJB equation, discretisation of control problems
(23 pages, 2002)

32. M. Krekel
Optimal portfolios with a loan dependent credit spread
Keywords: Portfolio optimisation, stochastic control, HJB equation, credit spread, log utility, power utility, non-linear wealth dynamics
(25 pages, 2002)

33. J. Ohser, W. Nagel, K. Schladitz
The Euler number of discretized sets – on the choice of adjacency in homogeneous lattices
Keywords: image analysis, Euler number, neighborhod relationships, cuboidal lattice
(32 pages, 2002)

34. I. Ginzburg, K. Steiner
Lattice Boltzmann Model for Free-Surface flow and Its Application to Filling Process in Casting
Keywords: Lattice Boltzmann models; free-surface phenomena; interface boundary conditions; filling processes; injection molding; volume of fluid method; interface boundary conditions; advection-schemes; upwind-schemes
(54 pages, 2002)

35. M. Günther, A. Klar, T. Materne, R. Wegener
Multivalued fundamental diagrams and stop and go waves for continuum traffic equations
Keywords: traffic flow, macroscopic equations, kinetic derivation, multivalued fundamental diagram, stop and go waves, phase transitions
(25 pages, 2002)

36. S. Feldmann, P. Lang, D. Prätzel-Wolters
Parameter influence on the zeros of network determinants
Keywords: Networks, Equicofactor matrix polynomials, Realization theory, Matrix perturbation theory
(30 pages, 2002)

37. K. Koch, J. Ohser, K. Schladitz
Spectral theory for random closed sets and estimating the covariance via frequency space
Keywords: Random set, Bartlett spectrum, fast Fourier transform, power spectrum
(28 pages, 2002)

38. D. d'Humières, I. Ginzburg
Multi-reflection boundary conditions for lattice Boltzmann models
Keywords: lattice Boltzmann equation, boudary condistions, bounce-back rule, Navier-Stokes equation
(72 pages, 2002)

39. R. Korn
Elementare Finanzmathematik
Keywords: Finanzmathematik, Aktien, Optionen, Portfolio-Optimierung, Börse, Lehrerweiterbildung, Mathematikunterricht
(98 pages, 2002)

40. J. Kallrath, M. C. Müller, S. Nickel
Batch Presorting Problems: Models and Complexity Results
Keywords: Complexity theory, Integer programming, Assigment, Logistics
(19 pages, 2002)

41. J. Linn
On the frame-invariant description of the phase space of the Folgar-Tucker equation
Key words: fiber orientation, Folgar-Tucker equation, injection molding
(5 pages, 2003)

42. T. Hanne, S. Nickel
A Multi-Objective Evolutionary Algorithm for Scheduling and Inspection Planning in Software Development Projects
Key words: multiple objective programming, project management and scheduling, software development, evolutionary algorithms, efficient set
(29 pages, 2003)

43. T. Bortfeld , K.-H. Küfer, M. Monz, A. Scherrer, C. Thieke, H. Trinkaus
Intensity-Modulated Radiotherapy - A Large Scale Multi-Criteria Programming Problem
Keywords: multiple criteria optimization, representative systems of Pareto solutions, adaptive triangulation, clustering and disaggregation techniques, visualization of Pareto solutions, medical physics, external beam radiotherapy planning, intensity modulated radiotherapy
(31 pages, 2003)

44. T. Halfmann, T. Wichmann
Overview of Symbolic Methods in Industrial Analog Circuit Design
Keywords: CAD, automated analog circuit design, symbolic analysis, computer algebra, behavioral modeling, system simulation, circuit sizing, macro modeling, differential-algebraic equations, index
(17 pages, 2003)

45. S. E. Mikhailov, J. Orlik
Asymptotic Homogenisation in Strength and Fatigue Durability Analysis of Composites
Keywords: multiscale structures, asymptotic homogenization, strength, fatigue, singularity, non-local conditions
(14 pages, 2003)

46. P. Domínguez-Marín, P. Hansen, N. Mladenovi´c , S. Nickel
Heuristic Procedures for Solving the Discrete Ordered Median Problem
Keywords: genetic algorithms, variable neighborhood search, discrete facility location
(31 pages, 2003)

47. N. Boland, P. Domínguez-Marín, S. Nickel, J. Puerto
Exact Procedures for Solving the Discrete Ordered Median Problem
Keywords: discrete location, Integer programming
(41 pages, 2003)

48. S. Feldmann, P. Lang
Padé-like reduction of stable discrete linear systems preserving their stability
Keywords: Discrete linear systems, model reduction, stability, Hankel matrix, Stein equation
(16 pages, 2003)

49. J. Kallrath, S. Nickel
A Polynomial Case of the Batch Presorting Problem
Keywords: batch presorting problem, online optimization, competetive analysis, polynomial algorithms, logistics
(17 pages, 2003)

50. T. Hanne, H. L. Trinkaus
knowCube for MCDM – Visual and Interactive Support for Multicriteria Decision Making
Key words: Multicriteria decision making, knowledge management, decision support systems, visual interfaces, interactive navigation, real-life applications.
(26 pages, 2003)

51. O. Iliev, V. Laptev
On Numerical Simulation of Flow Through Oil Filters
Keywords: oil filters, coupled flow in plain and porous media, Navier-Stokes, Brinkman, numerical simulation
(8 pages, 2003)

52. W. Dörfler, O. Iliev, D. Stoyanov, D. Vassileva
On a Multigrid Adaptive Refinement Solver for Saturated Non-Newtonian Flow in Porous Media
Keywords: Nonlinear multigrid, adaptive refinement, non-Newtonian flow in porous media
(17 pages, 2003)

53. S. Kruse
On the Pricing of Forward Starting Options under Stochastic Volatility
Keywords: Option pricing, forward starting options, Heston model, stochastic volatility, cliquet options
(11 pages, 2003)

54. O. Iliev, D. Stoyanov
Multigrid – adaptive local refinement solver for incompressible flows
Keywords: Navier-Stokes equations, incompressible flow, projection-type splitting, SIMPLE, multigrid methods, adaptive local refinement, lid-driven flow in a cavity
(37 pages, 2003)

55. V. Starikovicius
The multiphase flow and heat transfer in porous media
Keywords: Two-phase flow in porous media, various formulations, global pressure, multiphase mixture model, numerical simulation
(30 pages, 2003)

56. P. Lang, A. Sarishvili, A. Wirsen
Blocked neural networks for knowledge extraction in the software development process
Keywords: Blocked Neural Networks, Nonlinear Regression, Knowledge Extraction, Code Inspection
(21 pages, 2003)

57. H. Knaf, P. Lang, S. Zeiser
Diagnosis aiding in Regulation Thermography using Fuzzy Logic
Keywords: fuzzy logic,knowledge representation, expert system
(22 pages, 2003)

58. M. T. Melo, S. Nickel, F. Saldanha da Gama
Largescale models for dynamic multicommodity capacitated facility location
Keywords: supply chain management, strategic planning, dynamic location, modeling
(40 pages, 2003)

59. J. Orlik
Homogenization for contact problems with periodically rough surfaces
Keywords: asymptotic homogenization, contact problems
(28 pages, 2004)

60. A. Scherrer, K.-H. Küfer, M. Monz, F. Alonso, T. Bortfeld
IMRT planning on adaptive volume structures – a significant advance of computational complexity
Keywords: Intensity-modulated radiation therapy (IMRT), inverse treatment planning, adaptive volume structures, hierarchical clustering, local refinement, adaptive clustering, convex programming, mesh generation, multi-grid methods
(24 pages, 2004)

61. D. Kehrwald
Parallel lattice Boltzmann simulation of complex flows
Keywords: Lattice Boltzmann methods, parallel computing, microstructure simulation, virtual material design, pseudo-plastic fluids, liquid composite moulding
(12 pages, 2004)

62. O. Iliev, J. Linn, M. Moog, D. Niedziela, V. Starikovicius
On the Performance of Certain Iterative Solvers for Coupled Systems Arising in Discretization of Non-Newtonian Flow Equations
Keywords: Performance of iterative solvers, Preconditioners, Non-Newtonian flow
(17 pages, 2004)

63. R. Ciegis, O. Iliev, S. Rief, K. Steiner
On Modelling and Simulation of Different Regimes for Liquid Polymer Moulding
Keywords: Liquid Polymer Moulding, Modelling, Simulation, Infiltration, Front Propagation, non-Newtonian flow in porous media
(43 pages, 2004)

64. T. Hanne, H. Neu
Simulating Human Resources in Software Development Processes
Keywords: Human resource modeling, software process, productivity, human factors, learning curve
(14 pages, 2004)

65. O. Iliev, A. Mikelic, P. Popov
Fluid structure interaction problems in deformable porous media: Toward permeability of deformable porous media
Keywords: fluid-structure interaction, deformable porous media, upscaling, linear elasticity, stokes, finite elements
(28 pages, 2004)

66. F. Gaspar, O. Iliev, F. Lisbona, A. Naumovich, P. Vabishchevich
On numerical solution of 1-D poroelasticity equations in a multilayered domain
Keywords: poroelasticity, multilayered material, finite volume discretization, MAC type grid
(41 pages, 2004)

67. J. Ohser, K. Schladitz, K. Koch, M. Nöthe
Diffraction by image processing and its application in materials science
Keywords: porous microstructure, image analysis, random set, fast Fourier transform, power spectrum, Bartlett spectrum
(13 pages, 2004)

68. H. Neunzert
Mathematics as a Technology: Challenges for the next 10 Years
Keywords: applied mathematics, technology, modelling, simulation, visualization, optimization, glass processing, spinning processes, fiber-fluid interaction, trubulence effects, topological optimization, multicriteria optimization, Uncertainty and Risk, financial mathematics, Malliavin calculus, Monte-Carlo methods, virtual material design, filtration, bio-informatics, system biology
(29 pages, 2004)

69. R. Ewing, O. Iliev, R. Lazarov, A. Naumovich
On convergence of certain finite difference discretizations for 1D poroelasticity interface problems
Keywords: poroelasticity, multilayered material, finite volume discretizations, MAC type grid, error estimates
(26 pages,2004)

70. W. Dörfler, O. Iliev, D. Stoyanov, D. Vassileva
On Efficient Simulation of Non-Newtonian Flow in Saturated Porous Media with a Multigrid Adaptive Refinement Solver
Keywords: Nonlinear multigrid, adaptive renement, non-Newtonian in porous media
(25 pages, 2004)

71. J. Kalcsics, S. Nickel, M. Schröder
Towards a Unified Territory Design Approach – Applications, Algorithms and GIS Integration
Keywords: territory desgin, political districting, sales territory alignment, optimization algorithms, Geographical Information Systems
(40 pages, 2005)

72. K. Schladitz, S. Peters, D. Reinel-Bitzer, A. Wiegmann, J. Ohser
Design of acoustic trim based on geometric modeling and flow simulation for non-woven
Keywords: random system of fibers, Poisson line process, flow resistivity, acoustic absorption, Lattice-Boltzmann method, non-woven
(21 pages, 2005)

73. V. Rutka, A. Wiegmann
Explicit Jump Immersed Interface Method for virtual material design of the effective elastic moduli of composite materials
Keywords: virtual material design, explicit jump immersed interface method, effective elastic moduli, composite materials
(22 pages, 2005)

74. T. Hanne
Eine Übersicht zum Scheduling von Baustellen
Keywords: Projektplanung, Scheduling, Bauplanung, Bauindustrie
(32 pages, 2005)

75. J. Linn
The Folgar-Tucker Model as a Differetial Algebraic System for Fiber Orientation Calculation
Keywords: fiber orientation, Folgar–Tucker model, invariants, algebraic constraints, phase space, trace stability
(15 pages, 2005)

76. M. Speckert, K. Dreßler, H. Mauch, A. Lion, G. J. Wierda
Simulation eines neuartigen Prüfsystems für Achserprobungen durch MKS-Modellierung einschließlich Regelung
Keywords: virtual test rig, suspension testing, multibody simulation, modeling hexapod test rig, optimization of test rig configuration
(20 pages, 2005)

77. K.-H. Küfer, M. Monz, A. Scherrer, P. Süss, F. Alonso, A. S. A. Sultan, Th. Bortfeld, D. Craft, Chr. Thieke
Multicriteria optimization in intensity modulated radiotherapy planning
Keywords: multicriteria optimization, extreme solutions, real-time decision making, adaptive approximation schemes, clustering methods, IMRT planning, reverse engineering
(51 pages, 2005)

78. S. Amstutz, H. Andrä
A new algorithm for topology optimization using a level-set method
Keywords: shape optimization, topology optimization, topological sensitivity, level-set
(22 pages, 2005)

79. N. Ettrich
Generation of surface elevation models for urban drainage simulation
Keywords: Flooding, simulation, urban elevation models, laser scanning
(22 pages, 2005)

80. H. Andrä, J. Linn, I. Matei, I. Shklyar, K. Steiner, E. Teichmann
OPTCAST – Entwicklung adäquater Strukturoptimierungsverfahren für Gießereien Technischer Bericht (KURZFASSUNG)
Keywords: Topologieoptimierung, Level-Set-Methode, Gießprozesssimulation, Gießtechnische Restriktionen, CAE-Kette zur Strukturoptimierung
(77 pages, 2005)

81. N. Marheineke, R. Wegener
Fiber Dynamics in Turbulent Flows Part I: General Modeling Framework
Keywords: fiber-fluid interaction; Cosserat rod; turbulence modeling; Kolmogorov's energy spectrum; double-velocity correlations; differentiable Gaussian fields
(20 pages, 2005)

Part II: Specific Taylor Drag
Keywords: flexible fibers; k-ε turbulence model; fiber-turbulence interaction scales; air drag; random Gaussian aerodynamic force; white noise; stochastic differential equations; ARMA process
(18 pages, 2005)

82. C. H. Lampert, O. Wirjadi
An Optimal Non-Orthogonal Separation of the Anisotropic Gaussian Convolution Filter
Keywords: Anisotropic Gaussian filter, linear filtering, orientation space, nD image processing, separable filters
(25 pages, 2005)

83. H. Andrä, D. Stoyanov
Error indicators in the parallel finite element solver for linear elasticity DDFEM
Keywords: linear elasticity, finite element method, hierarchical shape functions, domain decom-position, parallel implementation, a posteriori error estimates
(21 pages, 2006)

84. M. Schröder, I. Solchenbach
Optimization of Transfer Quality in Regional Public Transit
Keywords: public transit, transfer quality, quadratic assignment problem
(16 pages, 2006)

85. A. Naumovich, F. J. Gaspar
On a multigrid solver for the three-dimensional Biot poroelasticity system in multilayered domains
Keywords: poroelasticity, interface problem, multigrid, operator-dependent prolongation
(11 pages, 2006)

86. S. Panda, R. Wegener, N. Marheineke
Slender Body Theory for the Dynamics of Curved Viscous Fibers
Keywords: curved viscous fibers; fluid dynamics; Navier-Stokes equations; free boundary value problem; asymptotic expansions; slender body theory
(14 pages, 2006)

87. E. Ivanov, H. Andrä, A. Kudryavtsev
Domain Decomposition Approach for Automatic Parallel Generation of Tetrahedral Grids
Key words: Grid Generation, Unstructured Grid, Delaunay Triangulation, Parallel Programming, Domain Decomposition, Load Balancing
(18 pages, 2006)

88. S. Tiwari, S. Antonov, D. Hietel, J. Kuhnert, R. Wegener
A Meshfree Method for Simulations of Interactions between Fluids and Flexible Structures
Key words: Meshfree Method, FPM, Fluid Structure Interaction, Sheet of Paper, Dynamical Coupling
(16 pages, 2006)

89. R. Ciegis , O. Iliev, V. Starikovicius, K. Steiner
Numerical Algorithms for Solving Problems of Multiphase Flows in Porous Media
Keywords: nonlinear algorithms, finite-volume method, software tools, porous media, flows
(16 pages, 2006)

90. D. Niedziela, O. Iliev, A. Latz
On 3D Numerical Simulations of Viscoelastic Fluids
Keywords: non-Newtonian fluids, anisotropic viscosity, integral constitutive equation
(18 pages, 2006)

91. A. Winterfeld
Application of general semi-infinite Programming to Lapidary Cutting Problems
Keywords: large scale optimization, nonlinear programming, general semi-infinite optimization, design centering, clustering
(26 pages, 2006)

92. J. Orlik, A. Ostrovska
Space-Time Finite Element Approximation and Numerical Solution of Hereditary Linear Viscoelasticity Problems
Keywords: hereditary viscoelasticity; kern approximation by interpolation; space-time finite element approximation, stability and a priori estimate
(24 pages, 2006)

93. V. Rutka, A. Wiegmann, H. Andrä
EJIIM for Calculation of effective Elastic Moduli in 3D Linear Elasticity
Keywords: Elliptic PDE, linear elasticity, irregular domain, finite differences, fast solvers, effective elastic moduli
(24 pages, 2006)

94. A. Wiegmann, A. Zemitis
EJ-HEAT: A Fast Explicit Jump Harmonic Averaging Solver for the Effective Heat Conductivity of Composite Materials
Keywords: Stationary heat equation, effective thermal conductivity, explicit jump, discontinuous coefficients, virtual material design, microstructure simulation, EJ-HEAT
(21 pages, 2006)

95. A. Naumovich
On a finite volume discretization of the three-dimensional Biot poroelasticity system in multilayered domains
Keywords: Biot poroelasticity system, interface problems, finite volume discretization, finite difference method
(21 pages, 2006)

96. M. Krekel, J. Wenzel
A unified approach to Credit Default Swaption and Constant Maturity Credit Default Swap valuation
Keywords: LIBOR market model, credit risk, Credit Default Swaption, Constant Maturity Credit Default Swap-method
(43 pages, 2006)

97. A. Dreyer
Interval Methods for Analog Circiuts
Keywords: interval arithmetic, analog circuits, tolerance analysis, parametric linear systems, frequency response, symbolic analysis, CAD, computer algebra
(36 pages, 2006)

98. N. Weigel, S. Weihe, G. Bitsch, K. Dreßler
Usage of Simulation for Design and Optimization of Testing
Keywords: Vehicle test rigs, MBS, control, hydraulics, testing philosophy
(14 pages, 2006)

99. H. Lang, G. Bitsch, K. Dreßler, M. Speckert
Comparison of the solutions of the elastic and elastoplastic boundary value problems
Keywords: Elastic BVP, elastoplastic BVP, variational inequalities, rate-independency, hysteresis, linear kinematic hardening, stop- and play-operator
(21 pages, 2006)

100. M. Speckert, K. Dreßler, H. Mauch
MBS Simulation of a hexapod based suspension test rig
Keywords: Test rig, MBS simulation, suspension, hydraulics, controlling, design optimization
(12 pages, 2006)

101. S. Azizi Sultan, K.-H. Küfer
A dynamic algorithm for beam orientations in multicriteria IMRT planning
Keywords: radiotherapy planning, beam orientation optimization, dynamic approach, evolutionary algorithm, global optimization
(14 pages, 2006)

102. T. Götz, A. Klar, N. Marheineke, R. Wegener
A Stochastic Model for the Fiber Lay-down Process in the Nonwoven Production
Keywords: fiber dynamics, stochastic Hamiltonian system, stochastic averaging
(17 pages, 2006)

103. Ph. Süss, K.-H. Küfer
Balancing control and simplicity: a variable aggregation method in intensity modulated radiation therapy planning
Keywords: IMRT planning, variable aggregation, clustering methods
(22 pages, 2006)

104. A. Beaudry, G. Laporte, T. Melo, S. Nickel
Dynamic transportation of patients in hospitals
Keywords: in-house hospital transportation, dial-a-ride, dynamic mode, tabu search
(37 pages, 2006)

105. Th. Hanne
Applying multiobjective evolutionary algorithms in industrial projects
Keywords: multiobjective evolutionary algorithms, discrete optimization, continuous optimization, electronic circuit design, semi-infinite programming, scheduling
(18 pages, 2006)

106. J. Franke, S. Halim
Wild bootstrap tests for comparing signals and images
Keywords: wild bootstrap test, texture classification, textile quality control, defect detection, kernel estimate, nonparametric regression
(13 pages, 2007)

107. Z. Drezner, S. Nickel
Solving the ordered one-median problem in the plane
Keywords: planar location, global optimization, ordered median, big triangle small triangle method, bounds, numerical experiments
(21 pages, 2007)

108. Th. Götz, A. Klar, A. Unterreiter, R. Wegener
Numerical evidance for the non-existing of solutions of the equations desribing rotational fiber spinning
Keywords: rotational fiber spinning, viscous fibers, boundary value problem, existence of solutions
(11 pages, 2007)

109. Ph. Süss, K.-H. Küfer
Smooth intensity maps and the Bortfeld-Boyer sequencer
Keywords: probabilistic analysis, intensity modulated radiotherapy treatment (IMRT), IMRT plan application, step-and-shoot sequencing
(8 pages, 2007)

110. E. Ivanov, O. Gluchshenko, H. Andrä, A. Kudryavtsev
Parallel software tool for decomposing and meshing of 3d structures
Keywords: a-priori domain decomposition, unstructured grid, Delaunay mesh generation
(14 pages, 2007)

111. O. Iliev, R. Lazarov, J. Willems
Numerical study of two-grid preconditioners for 1d elliptic problems with highly oscillating discontinuous coefficients
Keywords: two-grid algorithm, oscillating coefficients, preconditioner
(20 pages, 2007)

112. L. Bonilla, T. Götz, A. Klar, N. Marheineke, R. Wegener
Hydrodynamic limit of the Fokker-Planck-equation describing fiber lay-down processes
Keywords: stochastic dierential equations, Fokker-Planck equation, asymptotic expansion, Ornstein-Uhlenbeck process
(17 pages, 2007)

113. S. Rief
Modeling and simulation of the pressing section of a paper machine
Keywords: paper machine, computational fluid dynamics, porous media
(41 pages, 2007)

114. R. Ciegis, O. Iliev, Z. Lakdawala
On parallel numerical algorithms for simulating industrial filtration problems
Keywords: Navier-Stokes-Brinkmann equations, finite volume discretization method, SIMPLE, parallel computing, data decomposition method
(24 pages, 2007)

115. N. Marheineke, R. Wegener
Dynamics of curved viscous fibers with surface tension
Keywords: Slender body theory, curved viscous bers with surface tension, free boundary value problem
(25 pages, 2007)

116. S. Feth, J. Franke, M. Speckert
Resampling-Methoden zur mse-Korrektur und Anwendungen in der Betriebsfestigkeit
Keywords: Weibull, Bootstrap, Maximum-Likelihood, Betriebsfestigkeit
(16 pages, 2007)

117. H. Knaf
Kernel Fisher discriminant functions – a concise and rigorous introduction
Keywords: wild bootstrap test, texture classification, textile quality control, defect detection, kernel estimate, nonparametric regression
(30 pages, 2007)

118. O. Iliev, I. Rybak
On numerical upscaling for flow in heterogeneous porous media
Keywords: numerical upscaling, heterogeneous porous media, single phase flow, Darcy's law, multiscale problem, effective permeability, multipoint flux approximation, anisotropy
(17 pages, 2007)

119. O. Iliev, I. Rybak
On approximation property of multipoint flux approximation method
Keywords: Multipoint flux approximation, finite volume method, elliptic equation, discontinuous tensor coefficients, anisotropy
(15 pages, 2007)

120. O. Iliev, I. Rybak, J. Willems
On upscaling heat conductivity for a class of industrial problems
Keywords: Multiscale problems, effective heat conductivity, numerical upscaling, domain decomposition
(15 pages, 2007)

121. R. Ewing, O. Iliev, R. Lazarov, I. Rybak
On two-level preconditioners for flow in porous media
Keywords: Multiscale problem, Darcy's law, single phase flow, anisotropic heterogeneous porous media, numerical upscaling, multigrid, domain decomposition, efficient preconditioner
(18 pages, 2007)

122. M. Brickenstein, A. Dreyer
POLYBORI: A Gröbner basis framework for Boolean polynomials
Keywords: Gröbner basis, formal verification, Boolean polynomials, algebraic cryptoanalysis, satisfiability
(23 pages, 2007)

123. O. Wirjadi
Survey of 3d image segmentation methods
Keywords: image processing, 3d, image segmentation, binarization
(20 pages, 2007)

Status quo: July 2007